# Estimation of Hydrogen Production Rates from Radiolysable Material in Contact with Various Irradiated Fuels

**D. Bottomley[a], P. van Belle[b], D. Papaioannou[c], R. Nasyrov[d], V.V. Rondinella[e]**

**Abstract.** The storage of irradiated fuel is increasing as many installations are approaching their end-life and fuel or fuel-containing remnants from waste or samples are being placed in storage. Often these smaller experimental samples are mounted in epoxide resins or are placed containers with bitumen. It is particularly in combination with these radiolysable materials where the irradiation generates hydrogen that problems arise in longer term storage. The hydrogen generation results in either pressure build-up (with container bloating and eventual failure) or in case of gas release and mixture with air, a detonation. Previous work has examined the Phébus FPT1 bundle encased in resin where it was necessary for both transport and intermediate storage at Cadarache to assess this risk. This work is a first estimation of the radiolysis rates to be expected from various fuels and to assess the range of $H_2$ production from radiolysable material based on the results of the FPT1 Phébus bundle. The first step is to make a correlation of the total activity with the burn-up of $UO_2$ fuel. Then using the $H_2$ production rates measured for the Phébus fuel, an estimate of its dependence on fuel burn–up will be made and so help define the necessary design for the foreseen storage time.

## 1. INTRODUCTION

The Phébus FPT1 test was carried out in 1993 [1–3] and the bundle was embedded in epoxy resin and transported to ITU Karlsruhe for post-irradiation sectioning, examination and analysis. The return transport was now due but the licences for the available transport containers did not permit the casque's use for material that could radiolyse or thermolyse.

Therefore it was necessary to measure the radiolytic production of $H_2$ by the bundle segments by gas mass spectroscopy to support the safety case for the return transport (this was financed by the CEA). The intention of this paper is to model the dose rates and energy deposition in resin surrounding a bundle geometry with increasing burn-up and to combine this with the $H_2$ evolution measurements from the bundle to estimate resin radiolysis rates for resin-embedded irradiated fuel. This measurement could be used to support licensing of other such transports as well as the design considerations for storage of radioysable materials.

[a] EC-JRC-ITU Transuranium Institute, Germany
[b] EC-JRC-ITU Transuranium Institute, Germany
[c] EC-JRC-ITU Transuranium Institute, Germany
[d] EC-JRC-ITU Transuranium Institute, Germany
[e] EC-JRC-ITU Transuranium Institute, Germany

## 2. DESCRIPTION OF PHÉBUS FPT1 BUNDLE RADIOLYSIS ESTIMATES

### 2.1. **Gas mass spectroscopy of the specimens**

An estimate of the radiolysis of Phébus FPT1 bundle was required. A series of 5 discs that were not used in the post–irradiation examination and were therefore intact were chosen for testing. The position of the selected discs on the vertical tomography of the degraded bundle made directly after the FPT1 test is shown in Fig. 2.1 along with the cross-sectional tomographies of each of the remnant discs. The selected discs, that come from representative sections of the degraded bundle, were placed in an air-tight stainless steel container. Any hydrogen gas release resulting from degradation of the embedding resin would be measured by gas mass spectroscopy. The container was closed and then evacuated and back-filled with inert gas (Ar (5.0 purity - Air Liquide). A sample was taken and then the steel container was left for 69 days before a second sample of its atmosphere was taken. The 2 samples were then taken for analysis by gas mass spectroscopy.

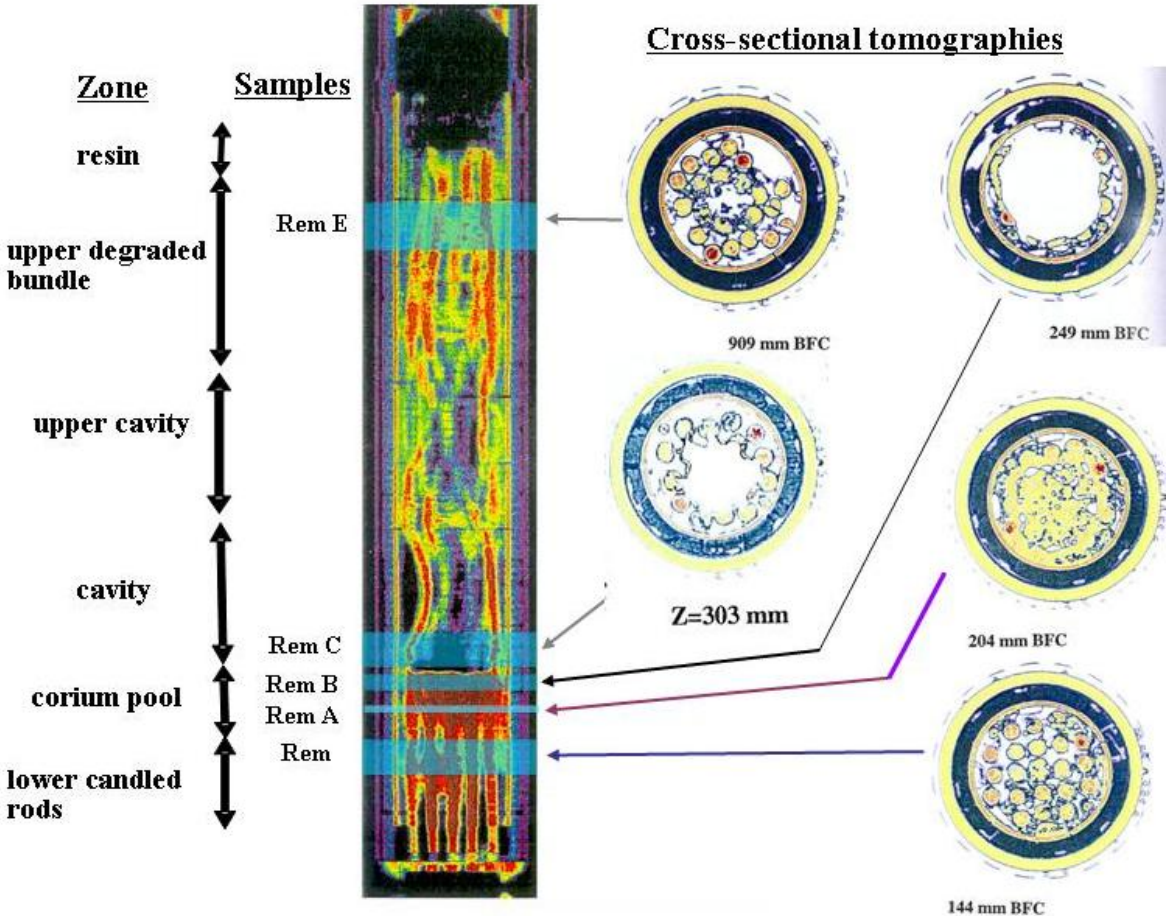


*FIG. 2.1. The positions of the 5 remnant discs used for gas analysis are shown on the sectional tomography of the degraded FPT1 bundle. On the left, the sections of the degraded bundle are indicated; on the right cross-sectional tomographies corresponding to the positions of the remnant discs are shown. These were used to estimate the cross-sectional area of the fuel and the resin at these heights of the bundle.*

The gas mass spectrograph was then calibrated with three certified Ar-$H_2$ mixtures with 1 ppm, 100 ppm and 1% $H_2$ content. The gas mass spectrographs (Balzers Omnistar MS) for the 2 gas samples (for the start and the end of the period) are shown in Fig. 2.2. The hydrogen content in the second sample taken from the container was then measured at 19,200 ppm + 20% (from all sources of

error). Therefore a value of (2±0.4)% (absolute) was determined. No fission gas (Kr and Xe) were observed in the spectrum, so that the fuel appears to be stable. Further details are given in Ref. [4].

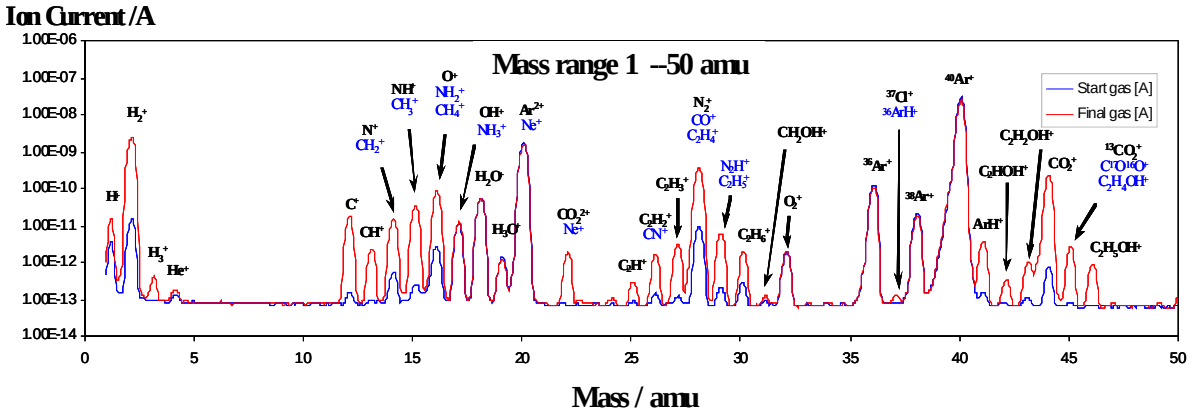


*FIG. 2.2. The initial gas mass spectrograph (in blue) and the final spectrum (in red) taken after 69 days. In addition to the Ar peak, some hydrocarbon residues, $N_2$, $O_2$ and $H_2$ are seen.*

## 2.2. **Estimation of fuel and resin masses**

It was next necessary to estimate the mass of fuel and reactor structural materials. This was done by using the linear density derived from tomograpic scans of the Phébus FPT1 bundle.

This linear mass graph is shown along with the tomography of the bundle after the FPT1 test in Fig. 2.3. The blue bars on the tomograph on the left show the positions of remnant discs used for the gas analysis. They are seen to have examples from a range of different bundle conditions: the upper degraded bundle (Rem E), cavity (Rem C), the corium pool and lower corium pool (Rem B and Rem A)) and finally the lower candled rods (Rem). On the right the discs are listed along with their average linear mass for the section they represent and an arrow showing the point on the graph. This is summarised in Table 2.1, and these values are used along with the thicknesses of the remnant discs to calculate the value for the mass of fuel and structural elements for the gas analysis samples (2872 g). In the final line the value for the whole bundle obtained by cross-multiplying all the discs thicknesses by the corresponding linear mass for that bundle section is given (14366 g).

TABLE 2.1. POSITIONS, THICKNESSES AND FUEL MASSES OF ALL REMNANT DISCS ANALYSED BY GAS ANALYSIS FOR $H_2$ RADIOLYSIS AS WELL AS THE TOTAL BUNDLE MASS

| Remnant and height above bottom of fuel | Area of bundle | Thickness of disc [mm] | Linear mass [g·mm$^{-1}$] | Mass of fuel in remnant [g] |
|---|---|---|---|---|
| Rem E @ 909 mm | Upper degraded bundle | 52.5 | 15 | 787.5 |
| Rem C @ 303 mm | cavity | 62 | 8.5 | 527 |
| Rem B @ 249 mm | corium pool | 20.1 | 17 | 341.7 |
| Rem A @ 204 mm | Lower corium pool | 13.5 | 26 | 351 |
| Rem @ 144 mm | Lower candling rods | 42.2 | 20.5 | 865.1 |
| Total estimated fuel and structural elements for sample | | | | 2872.3 |
| Total estimated fuel and structural elements for FPT1 bundle | | | | 14366 |

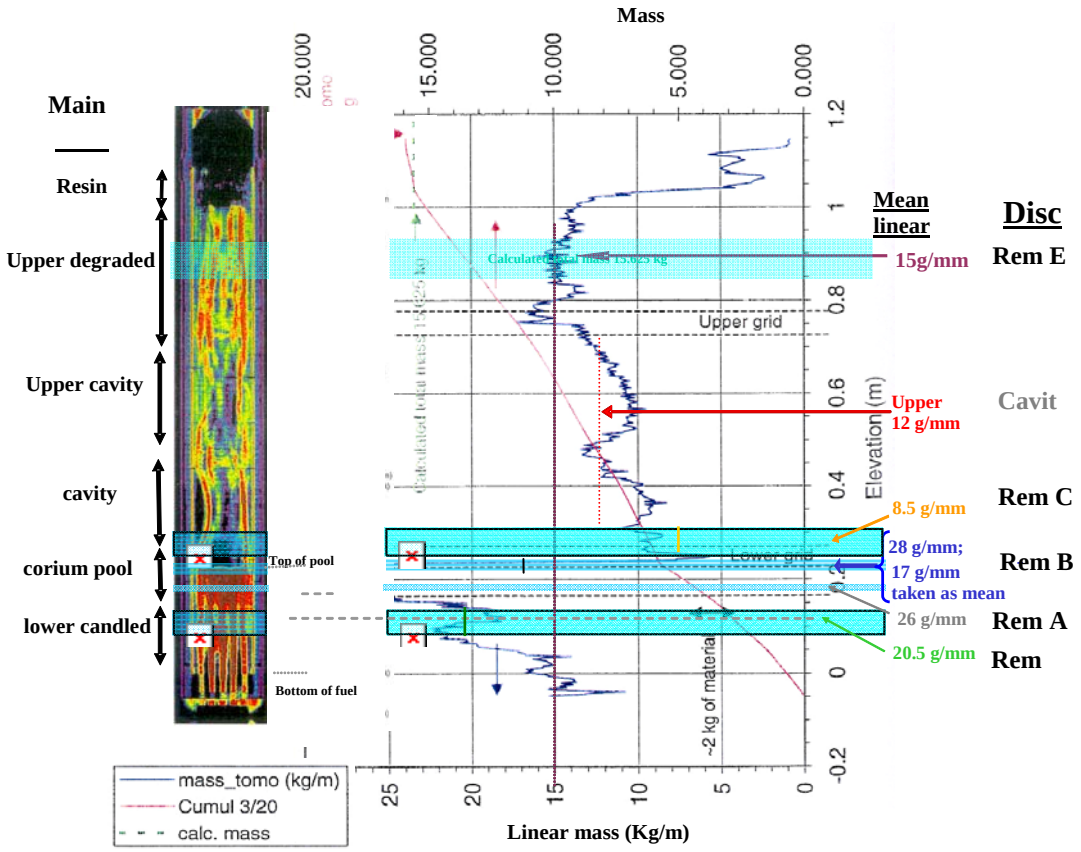


*FIG. 2.3. Diagram giving the linear masses of the various remnants of the FPT1 bundle that have been selected for analysis of $H_2$ gas evolution along with their position in the bundle.*

### *2.2.2. Volume of resin per remnant disc*

The calculations for the resin volume and the melt (fused fuel, cladding and structural material) for each disc are based on the cross-section of the 20 rod FPT1 bundle with a central Ag-In-Cd control rod combined with the thicknesses of the discs. Estimates are based on original fuel rod geometry and cross sections and then adapted for swelling of rods and missing rods in upper part, and for resin – filled cavities, corium and rod cross-sections in the lower part. The various estimates were assessed using the cross-sectional tomographs given in Fig. 2.3.

Thus Rem C as part of the central cavity was estimated as having only an 8 mm wide thick outer ring of material with 10% porosity in order to calculate the percentage of cross-section as melt and that of free volume filled with resin. By contrast Rem E from the upper bundle was calculated as having a cross-section equivalent to having one rod extra in cross-section for half its height. More details are given in Ref. [4].

This enabled the volume of resin for the remnants used for gas analysis to be estimated and then the total volume of the resin in the FPT1 bundle; this was found to be 449 cm³ volume of resin for the remnants and 2872 cm³ for the FPT1 bundle. The free volume in the autoclave containing the segments was 920 cm³. The concentration of H2 in the container was 2% (±0.4%) after 69 days. From this the H2 release rate for the resin in the remnants calculated and hence releases could be estimated for the whole FPT1 bundle as 1.65±0.33 cm³ of $H_2$ per day. This gives 0.000594 cm³ $H_2$/day/cm³ resin (or $9.89 \times 10^{-5}$ cm³ H2/day/g $UO_2$ fuel of 23.4 GW·d·$t^{-1}UO_2$ BU). The current estimates of the FPT1 bundle activity (total Cs-137 activity ~$4.10^{12}$ Bq) show that it is at a steady level. Therefore radiation doses will not be expected to change much with time.

TABLE 2.2. ESTIMATED PARTITION BETWEEN RESIN AND FUEL FOR EACH OF THE DISCS USED IN THE TEST, ALONG WITH NOTES OF THE BUNDLE'S AND FUEL ROD'S DIMENSIONS

| Zone | Remnants | Partition | | Linear mass (see Fig. 2.2) |
|---|---|---|---|---|
| | | Fuel [%] | Resin [%] | [g·mm$^{-1}$] |
| Lower candled rods | Rem | 40 | 60 | 20.5 |
| Corium pool | Rem - A | 95 | 5 | 26 |
| Cavity/corium pool | Rem - B | 65 | 35 | 17 |
| Cavity | | 36 | 64 | 8.5 |
| Upper cavity | Rem -C | 20 | 80 | 12 |
| Upper bundle | Rem -E | 34 | 66 | 15 |
| Resin | | 20 | 80 | 2 |

Notes

1) Thoria sheath: 73 mm int. dia., fuel cladding ~9.5 mm ext. dia.
2) Bundle configuration: 20 rods, 1 control rod and guide tube (ext. dia. 12.1 mm) and 2 ultrasonic thermometers (ext. dia. 6 mm).
3) 'Free' cross-section calculation: $ThO_2$ cross-section = $\pi(73/2)^2$ mm$^2$ = 41.854 cm². Rods cross-section = $[20.\pi(9.5/2)^2 + \pi(12.1/2)^2 + 2.\pi(6/2)^2]$ mm$^2$ =15.891cm². The difference is 25.96 cm² or 62.0% of the cross-section will be filled with resin for a bundle in its initial condition.

# 3. RADIOLYSABLE MATERIAL TRANSPORT AND STORAGE CONSIDERATIONS

## 3.1. **Transport**

Assuming that the container is filled with an inert atmosphere (eg. $N_2$) directly after loading then this will greatly reduce risk and power of any deflagation (typically Type B containers are air-tight and capable of being inerted).

In addition to back-filling the transport container with inert atmosphere, one can ensure a large free volume to take up the releases, or to have a catalytic recombiner system in the container to getter the evolved $H_2$ or have an inert gas in the inner sealed container.

## 3.2. **Storage - additional requirements**

This problem also applies to all irradiated fuel due for storage where it is not possible to separate all the radiolysable material from the fuel. There are additional requirements that the inner containers are capable of atmosphere evacuation and back-filling with inert gas as well as the transport container. The licence for the Phébus FPT1 bundle storage at CEA (being applied for at the same time as the transport licence) required that there would be no pressure build-up in the inner containers. Hence, outer containers were constructed with open apertures and inner containers with poral filter apertures in order to avoid any pressure build-up while minimising contamination through the filters. Hence avoiding pressure-build-up was the first priority.

# 4. ESTIMATION OF RADIATION

## 4.1. **Data format**

The modelling was performed with ORIGEN for a 17 × 17 Westinghouse PWR bundle. The neutron data was given in neutrons per sec per metric tonne U metal (Mt U). This was sub-divided into:

1) α, n neutrons;
2) spontaneous fission neutrons;
3) delayed neutrons (which were zero when fission had ceased).

The total neutron (in neutrons per sec per Mt U) was also given for various energy ranges and each class could be cross-multiplied with its mean energy and the total neutron energy estimated in MeV per sec per Mt U.

The gamma information was given as the gamma energy release rates in MeV per sec per Mt U for each energy range as well as for the total gamma energy range.

In addition the total power (Watt per Mt U) from all sources - neutrons, alpha, beta and gamma was also given. The alpha and beta is not given directly, so an estimate of this is made by deduction of neutron and gamma energy from the total power. Finally a conversion from MeV per sec per Mt U to Watt per Mt U (equals J per sec per Mt U) was performed multiplying by $1.602 \times 10^{-13}$, while a conversion from tonne U metal to tonne of $UO_2$ was made by dividing by 0.88.

## 5. ESTIMATION OF RADIOLYSIS RATES

### 5.1. **Density assumptions**

It was assumed that 10 tonnes of U are embedded in 1 tonne of resin. Estimates needed to be made concerning the porosity; here the density of the epoxide resin is taken as 1.20 $g \cdot cm^{-3}$ [5].

The value of $\rho UO_2 \sim 9.90$ $g \cdot cm^{-3}$ was assumed. This corresponds to the full theoretical density of $UO_2$ of 10.8 $g \cdot cm^{-3}$ at 92.5% density. This value yields the following volume ratios: 45.2 vol.% resin and 54.8 vol.% $UO_2$. This does not vary greatly as can be seen in Tale 5.1 below: there is only a variation of 2% in 45% ( or ~4% relative for a 3 times increase in porosity).

TABLE 5.1. $UO_2$ DENSITY AND VOLUME RATIOS FOR FUEL AND RESIN WITH VARIATION OF FUEL POROSITY

| Fuel porosity [%] | Rel. fuel density [%] | Effective density $UO_2$ fuel(*) [$g \cdot cm^{-3}$] | Volume resin [%] | Volume fuel [%] |
|---|---|---|---|---|
| 5 | 95 | 10.00 | 45.4 | 54.6 |
| 7.5 | 92.5 | 9.90 | 45.2 | 54.8 |
| 15 | 85 | 9.18 | 43.3 | 56.7 |

(*) theoretical $\rho_{UO2}$ (@ 100% density) = 10.8 $g \cdot cm^{-3}$

#### *5.1.1. Geometry*

The fuel rod geometry assumed that 4 quarter rods (of each 10 mm dia.) were sited on each corner of a 15 × 15 mm square. This geometry corresponds to that of the rods in FPT1 bundle at the start of the experiment. However tomographic sections of FPT1 in Figs. 2.1–2.2 show that there is considerable deformation; the upper bundle has lost rods or they have swollen and/or have slumped together. The pool is a quite different geometry and the lower bundle also has additional rivulets of molten material candling down the rods. Therefore this geometry serves only as a rough estimate.

#### *5.1.2. Deposition of power in the total mass*

Given the high stopping power of the polymeric material for neutrons compared to the heavy metal present in the fuel, a division for the power deposition for neutrons was taken as 10% for fuel and 90% for resin.

For the power deposition for gamma it was assumed that was twice as much gamma being absorbed by the fuel compared to neutron radiation). This resulted in a division of 20% deposited in the fuel and 80% in the resin.

The deposition of power for alphas and beta between the fuel and the resin assumed an α-penetration 40 μm into resin (as with water). However the problem was what to allow for beta given that it can penetrate thin steel or several centimeters of water or resin. As alpha radiation is estimated to cause 1000 times more ionisation than betas it was proposed to increase the 'effective range' of the alpha radiation to 50 μm to allow for this. This 10 μm increase would roughly compensate for 1 cm of beta radiation penetration. Using the starting rod geometry indicated in the previous section, this would give a ratio of cross-sectional area of resin compared to the total area in the bundle that would be penetrated by alpha and beta radiation as, $0.50025 \times \pi/25(9-\pi) = 0.010733$; thus it would penetrate approximately 1% by volume of the resin. However as the interface is likely to be the site of stresses and pre-existing cracks and hence accelerate the degradation, it was proposed to multiply this by a factor 10 to allow for this. Thus an estimate of 10% alpha and beta energy deposition in the resin was adopted. These values are summarised in Table 5.2 below.

TABLE 5.2. SUMMARY OF THE RATIOS OF POWER DEPOSITION BETWEEN FUEL AND RESIN FOR THE VARIOUS RADIATION SOURCES

| Fuel-resin power division | Radiation | Fuel | Resin |
|---|---|---|---|
| 1/10 & 9/10 | neutron | 0.1 | 0.9 |
| 2/11 & 9/11 | gamma | 0.2 | 0.8 |
| See Sect. 5.1.1 & 5.1.2 | α, β | 0.9 | 0.1 |

## 5.2. **Initial comments**

Initially it was noted that the total power (gamma + beta + alpha + neutron power) per Mt U immediately after reactor shutdown, ie. with no cooling period, is insensitive to burn-up as most of the power immediately after shutdown comes from the very short-lived nuclides and their concentration will quickly reach equilibrium when a reactors runs for a few days; at higher burn-ups their concentration does not significantly increase because they decay as fast as they are created. By contrast, the total power after a five year cooling period does increase. Now there are only long-lived nuclides remaining and their concentration builds up with rising burn-up. No great differences between PWR and BWR conditions were anticipated.

## 5.3. PROPORTION OF POWER DEPOSITED IN RESIN AND FUEL

### *5.3.1. Total power distribution in resin*

Fig. 4 shows the total power deposition in the resin and fuel and it is seen that the resin receives close to 30% of the total power. There is a slow exponential growth that could be locally interpolated with a linear function.

### *5.3.2. Neutron power distribution*

As can be seen in Fig. 5.2, the majority (91%) of the power from neutrons is deposited in resin as was assumed earlier. It is also seen that it is very small compared to gamma but that it is growing exponentially with burn-up; it increase by 104 times in going to 60 $GW \cdot d \cdot t\ UO_2$, but still represents less than 1 in 106 of the total power deposition (~0.001 $W \cdot t^{-1}\ UO_2$ vs. $10^3\ W \cdot t^{-1}\ UO_2$).

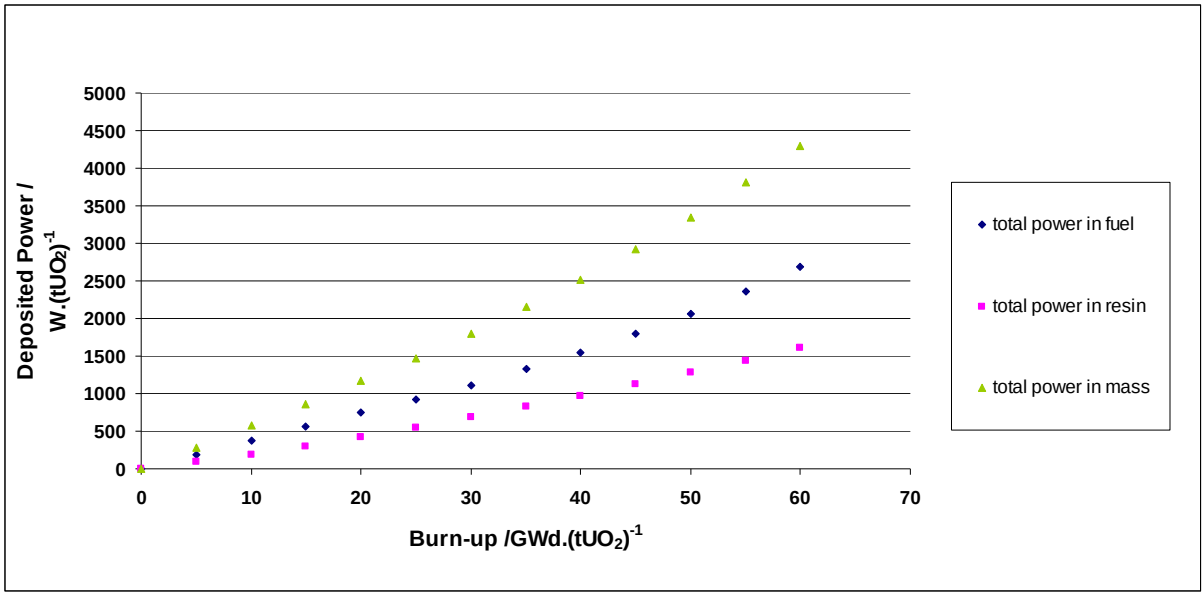


*FIG. 5.1. Total power deposition in resin and fuel with burn-up after a 5 year cooling time.*

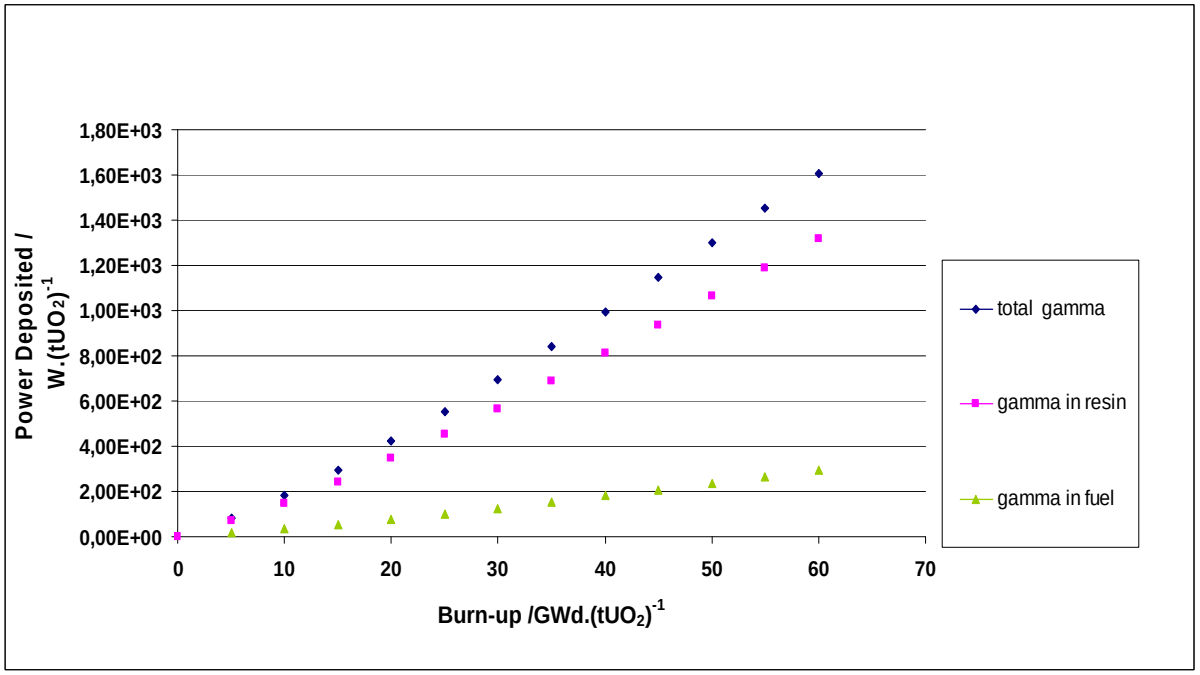


*FIG. 5.2. Neutron power distribution in resin and fuel with burn-up after a 5 year cooling time.*

### *5.3.3. Gamma power distribution*

The gamma power distribution between can be seen in Fig. 5.3. However very large total powers (~1 $kW \cdot t^{-1}$ $UO_2$) are seen and there is a slow exponential growth of this source of deposited power with burn-up. If a line is extrapolated from about 23 $GW \cdot d \cdot t^{-1}$ $UO_2$ then it is seen that there is an underestimate of about 18% for gamma power deposition in resin at 60 $GW \cdot d \cdot t^{-1}$ $UO_2$.

### *5.3.4. Alpha and beta power distribution*

The estimate was that 10% of the alpha and beta power was deposited in the resin and it is calculated approximately by deduction of gamma and neutron power from the total power. Again as a

consequence of the overall exponential growth of the total power this is reflected in a slow exponential (practically linear) growth of estimated alpha and beta power deposited in the resin with burn-up in Fig. 5.4.

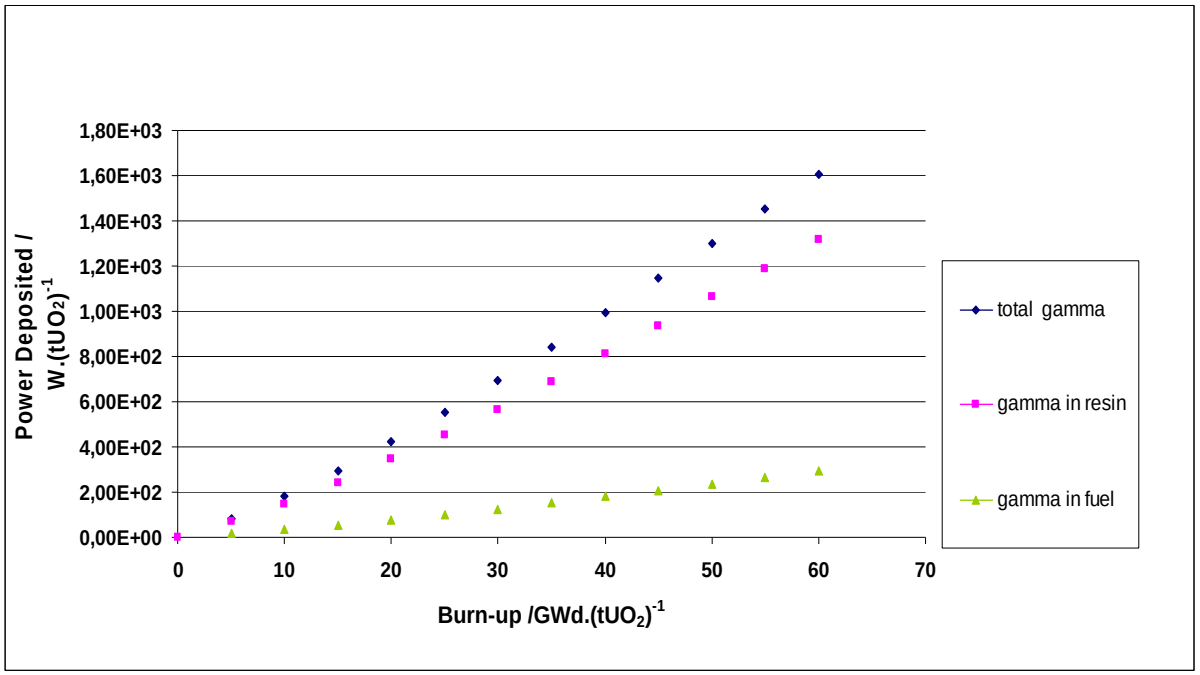


*FIG. 5.3. Gamma power deposition in resin and fuel with burn-up after a 5 year cooling time.*

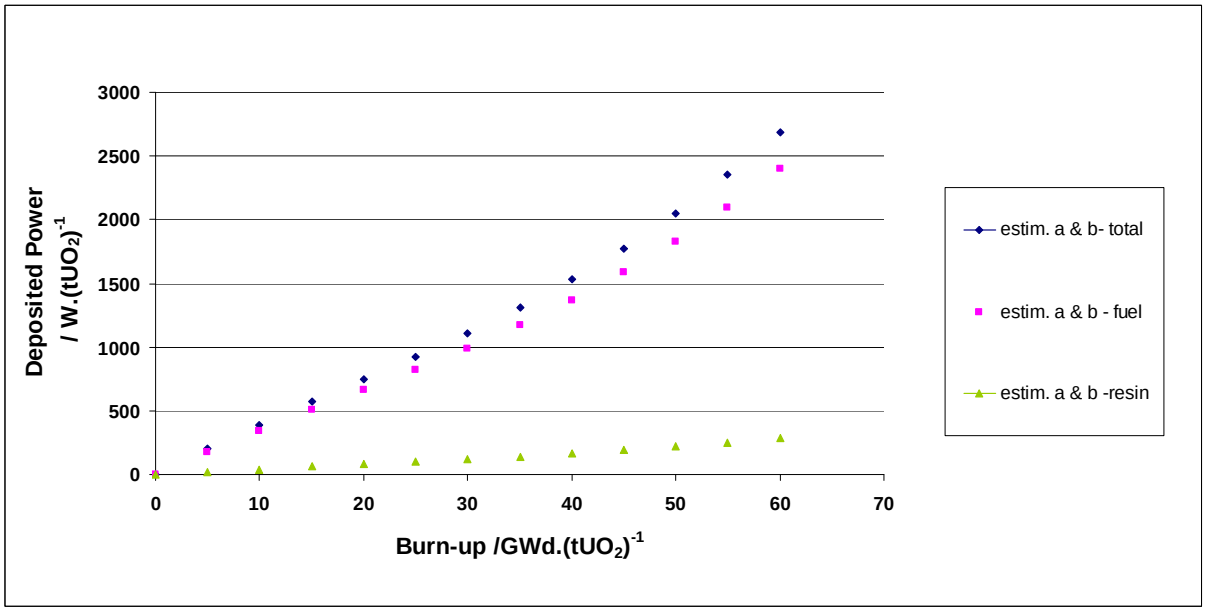


*FIG. 5.4. Alpha and beta power deposition in resin and fuel with burn-up after a 5 year cooling time.*

However the power deposition from alpha and beta in resin is ~300 $W \cdot t^{-1}$ $UO_2$ at a burn-up of 60 $GW \cdot d \cdot t^{-1}$ $UO_2$ is lower than that from gamma and represents about a quarter of the gamma power deposited.

## 5.4. EFFECT OF VARYING THE NEUTRON POWER DEPOSITION IN RESIN

Since the gamma power is the major source of power deposited in the resin. The variation of the assumed gamma repartition between fuel and resin was also examined. Here the division of the gamma power deposition between fuel and resin was varied between 5% in fuel and 95% in resin to 30 % in fuel and 70% in resin. The results are shown in Fig. 5.5 for low burn–up (5 GW·d·t$^{-1}$ $UO_2$) and high burn-up fuel (60 GW·d·t$^{-1}$ $UO_2$).

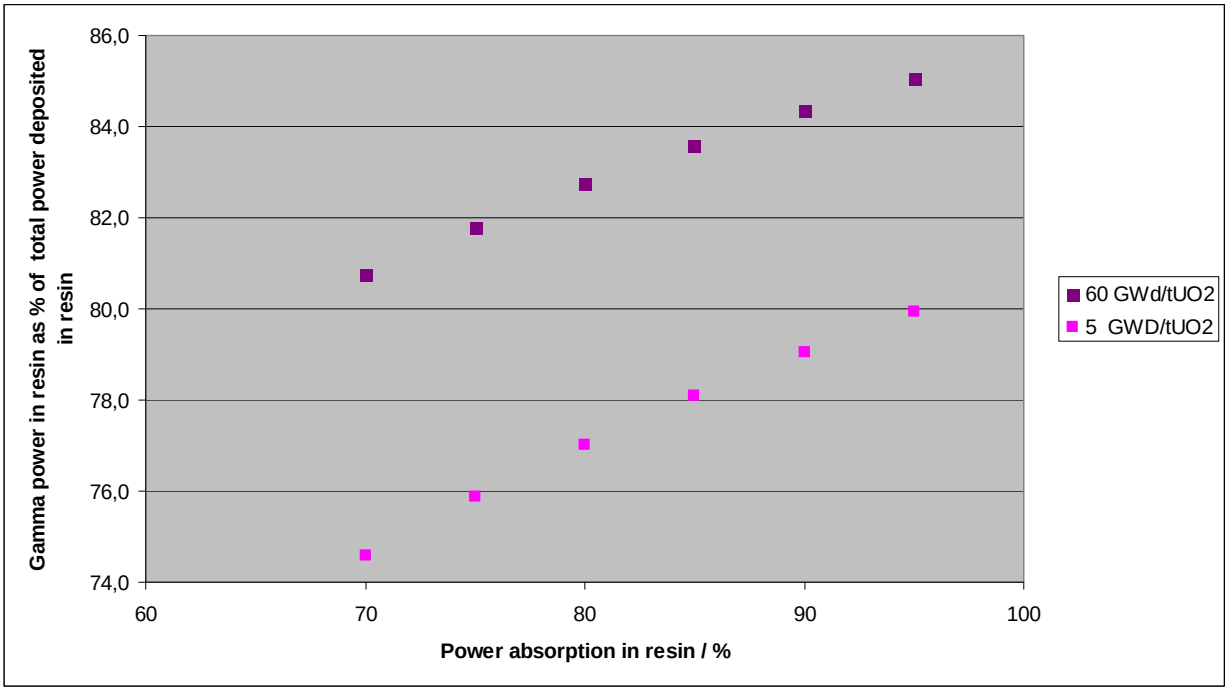


*FIG. 5.5 Variation of gamma power deposited in resin as a percentage of total deposited power in resin with division of gamma power deposition from 30% fuel -70% resin to 5 % fuel and 95% resin for a high and low burn-up fuel after a 5 year cooling time.*

They show that the total power deposited increases with burn-up and that the variation in total gamma power deposited in resin (as percentage of the total deposited power) is quite small. Thus at the low burn-up 5 GW·d·t$^{-1}$ $UO_2$ (the most sensitive case) the gamma power deposited in resin is 75% of the total deposited power in resin when only 70 % of gamma is deposited in resin but rises to 80% of the total deposited power in resin when 95% of the gamma is deposited in resin. For high BU 60 GW·d·t$^{-1}$ $UO_2$ fuel the corresponding statistics are 81% of the total power is deposited in resin from gamma at 70% of gamma deposition in resin; this rises to gamma being 85% of the total deposited power in resin when a division of the gamma power of 95% in resin and 5% in fuel is used. Both these figures represent a variation of ~5% of total power over the range of deposition ratios. A slow reduction in this variation is seen with burn-up – presumably because the total power deposited is rising steadily.

## 5.5. CALCULATION OF HYDROGEN RELEASES

This is based on the geometrical values of the Phébus FPT1bundle and the proportions selected for the power deposition between resin and fuel. The experimental value of the Phébus FPT1 bundle discs was given as 2.0% $H_2$ ± 0.4% $H_2$ (absolute) concentration in 69 days. This leads to an estimate of 1.65 (± 0,33) cm³ of $H_2$ per day for the entire FPT1 bundle; (ie from 1.32–1.98 cm³·d$^{-1}$). This gives 0.000594 cm³ $H_2$ per day per cm³ resin, or (or 9.89 × 10$^{-5}$ cm³ $H_2$ per day per g $UO_2$ fuel of 23.4 GW·d·t$^{-1}$ $UO_2$ BU). The major contribution after a 5 year cooling period is gamma radiation at

approximately 75–80% (see Sect. 5.4).

For transport and for intermediate storage conditions, the profile for gamma power deposition in resin is considered to be the best estimate of the radiolysis rates for resin in an irradiated fuel bundle. Therefore a linear extrapolation with a percentage addition has been taken. This linear percentage addition is based on the radiolysis value obtained for the Phébus FPT1 embedded bundle at 23.4 $GW \cdot d \cdot t^{-1}$ $UO_2$. As stated earlier this excess over the linear extrapolation was 18% at 60 $GW \cdot d \cdot t^{-1}$ $UO_2$ therefore a rounded value of 20% excess at 60 $GW \cdot d \cdot t^{-1}$ $UO_2$ in addition to the linear extrapolation was chosen. Thus the estimate for radiolysis rates of resin-embedded irradiated fuel of 40–60 $GW \cdot d \cdot t^{-1}$ $UO_2$ burn-up was estimated as follows:

- a factor of (40/23.4) × 1.10 for a 40 $GW \cdot d \cdot t^{-1}$ $UO_2$ = 1.88
- a factor of (50/23.4) × 1.15 for a 50 $GW \cdot d \cdot t^{-1}$ $UO_2$ = 2.46
- a factor of (60/23.4) × 1.20 for a 60 $GW \cdot d \cdot t^{-1}$ $UO_2$ = 3.08

This yields radiolysis rates for resin surrounding UO2 fuel in a bundle geometry as given in Table 5.3 below:

TABLE 5.3. RADIOLYSIS ESTIMATES FOR $UO_2$ IRRADIATED FUELS FOR A RANGE OF BURN-UPS FROM 23–60 $GW \cdot d \cdot t^{-1}$ $UO_2$

| Fuel BU [$GW \cdot d \cdot t^{-1}$ $UO_2$] | Factor for increase | Radiolysis rate [$cm^3$ $H_2$/day/$cm^3$ resin] | Error (±30%)(*) |
|---|---|---|---|
| 23.4 | 1 | 0.000594 | ±0.000178 |
| 40 | (40/23.4) × 1.10 = 1.88 | 0.00112 | ±0.000335 |
| 50 | (50/23.4) × 1.15 = 2.46 | 0.00146 | ±0.000438 |
| 60 | (60/23.4)× 1.20 = 3.08 | 0.00183 | ±0.000548 |

(*) Accuracy is ±30% (20% on experimental value and 10% on modelling), assuming other factors are similar (i.e. accuracy under optimum conditions).

The accuracy of the radiolysis measurement was given as 20% relative [1], it was proposed to add an additional error of 10% for the extrapolation as the best possible. This estimate must be seen in the context that many estimated parameters relating the fuel-resin geometry and exact volumes of resin incorporated in the fuel are not well known and that individual assessments are made in each case. Here the main sources of errors can be established and specific calculations made to check the error levels or scoping calculations to verify the sensitivity of key parameters.

## 6. CONCLUSIONS

1) Gamma power appears to be the main source deposited in resin at about 80% and shows a slow exponential growth with burn-up at a cooling period of 5 years.
2) Alpha annd beta radiation are then the next major source at ~20%, but are the most poorly characterized.
3) Neutron deposited energy appears to increase the most with increasing burn-up but remains after a 5 years cooling period only a minor source at 10–7 %. Its contribution could become more important in longer time frames which would need further studies.
   MOX fuel would not be expected to very different in a similar study but the larger role of the neutron power could be significant for long term cooling times (or repository studies).
4) Estimates of hydrogen generation have been made for fuel from 40–60 $GW \cdot d \cdot t^{-1}$ $UO_2$ burn-up on the basis of the modelling of gamma power deposition in resin. These rates vary from 0.00059–0.002 $cm^3$ $H_2$/day/$cm^3$ resin in going from 23.4–60 $GW \cdot d \cdot t^{-1}$ $UO_2$ burn-up. Accuracy is expected to be ±30% under the most similar (i.e. optimum) cases.

5) Varying the proportion of gamma power deposited in resin (as the major source) between 70–95% of gamma power being deposited in resin showed a slight variation of total power deposited in resin and indicates that it is not a critical parameter.
6) These sorts of calculations can assist in transport licensing and design considerations of storage for irradiated radiolysable material.

## REFERENCES

[1] VON DER HARDT, P., JONES, A.V., LECOMTE, C., TATTEGRAIN, A., Nuclear safety research. The Phebus FP severe accident experimental programme, Nuclear Safety **35** (2) (1994) 187–205.
[2] SCHEURER, H., CLEMENT, B., PHEBUS FP Data Book FPT1, Document PH-PF IS/92/49, (1997).
[3] JACQUEMAIN, D., BOURDON, S., DE BRAEMECKER, A., BARRACHIN, M., Phébus PF – FPT1 Final Report, IPSN Tech. Report No. IP/00/479, (2000).
[4] BOTTOMLEY, D., PAPAIOANNOU, D., NEU, J.-M., UHLIG, M., GLATZ, J.-P., WEGEN, D, CARBOL, P., FORS, P., RONDINELLA, V.V., SIMONDI-TEISSEIRE, B., JOUDON, A., Obtaining a licence for transporting radiolysable material, 47th Annual Workshop of the Working Group 'Hot Laboratories & Remote Handling', RIIAR, Dimitrovgrad (2010).
[5] PANG, K.T., GILLHAM, J.K., Anomalous Behaviour of Cured Epoxy Resins: Density at Room Temperature vs. Time and Temperature of Cure, Tech. Rep. No. 15, (contr No. N00014-84-K-0021), Polymer Materials Program, Dept of Chemical Engineering, Princeton University, Princeton (1988).